Self-sustained double-diffusive interleaving

ALESSANDRO STOCCHINO†

Dipartimento di Ingegneria delle Costruzioni, dell'Ambiente e del Territorio, University of Genova,
via Montallegro 1, 16145 Genova, Italy

The formation and evolution of double-diffusive interleaving is experimentally investigated with the purpose of analysing the influence of the convective flow structures, at different scales, on the mean flow. Recently, Krishnamurti (*J. Fluid Mech.*, vol. 558, 2006, p. 113) has shown that, in the case of a continuous stratification experiment, the Reynolds stresses, due to convective flow patches, are able to vertically transport horizontal momentum, maintaining the mean flow. This mechanism is similar to the *turbulent wind* observed in thermal convection. In this study, the interleaving is produced using the classical set-up of Ruddick & Turner (*Deep-Sea Res.*, vol. 558, 1979, p. 903). The dam-break experiments better resemble the case of oceanic fronts, where interleaving is commonly observed. The flow structures are investigated by measuring the two-dimensional flow fields using the particle image velocimetry technique. The resulting two-dimensional vector fields reveal complex fine-scale flow structures, and convective patterns are observed inside the finger-favourable layers. Vortical structures at scales comparable with the layer thickness are embedded in these regions and seem to be responsible for sustaining the horizontal mean flow against the viscous dissipations, especially in a region close to the layer nose. A spectral analysis of the flow fields suggest that the energy balance is governed by an inverse energy cascade, which implies a transfer of energy from the smaller scales to the larger scales (mean flow).

Key words: buoyancy-driven instability, double-diffusive convection

---

1. Introduction

The occurrence of double-diffusive interleaving in oceanic fronts and confluence zones is well documented in the oceanographic literature (see Ruddick & Richards 2003, for a review). The role of the thermohaline intrusions in the transport of heat and salt is often invoked to explain the formation of thermal inversion measured via CTD (conductivity, temperature, depth) recordings. Intrusions are most likely to occur near fronts, where the spatial variability of the physical characteristics (temperature and salinity) of the water masses are more pronounced. Examples are found at the Mediterranean outflow, tropical and subtropical Pacific regions, and at the Antarctic, where intrusions are thought to be an important aspect in the formation of the Antarctic bottom water. Furthermore, horizontal intrusions and the consequent enhanced lateral fluxes cause the decay of large-scale vortical structures like Meddies and rings, such as the Gulf Stream ring (see Ruddick & Richards 2003, and references therein).

† Email address for correspondence: jorma@dicat.unige.it

Owing to its relevance, double-diffusive interleaving has been extensively studied both theoretically (see Stern 1967; Toole & Georgi 1981; Holyer 1983; Niino 1986; Ruddick & Kerr 2003, among others) and experimentally (e.g. Ruddick & Turner 1979; Holyer *et al.* 1987; Ruddick, Phillips & Turner 1999; Krishnamurti 2006; Griffiths & Bidokhti 2008).

Holyer (1983) has theoretically proved that a fluid with a vertical and horizontal distribution of salt and temperature, with horizontal gradients that compensate each other to ensure that the isophycnals are essentially horizontal, is linearly unstable for any values of the horizontal gradients of the two components. The resulting motion takes the form of a sequence of layers that alternately move in opposite directions. If we consider a single layer, it has been observed that one interface is unstable in a finger sense, whereas the opposite one is unstable in a diffusive sense (see Ruddick & Turner 1979; Holyer *et al.* 1987, among others). In particular, below the layer that carries fluid with an excess of salt, we expect salt fingers to occur.

Ruddick (2003) has published an exhaustive and stimulating review of the numerous experimental work regarding thermohaline intrusions. He discussed several experimental configurations used to produce horizontal intrusions, trying to summarize the main outcomes of more than three decades of research. Recurrent questions can be found in most of the cited works regarding, in particular, the driving mechanism of the horizontal intrusions, the typical vertical length scale of the layers and the nose velocity. In most of these studies, the vertical layer spacing was found to be proportional to the ratio of the property anomaly with the density gradient. Agreement is also found in the dependence of the nose velocity on the buoyancy frequency and the layer thickness. As a possible driving mechanism of the intrusions, Ruddick & Turner (1979) proposed a dynamical argument based on the energy balance of a sequence of layers, where the salt-finger-buoyancy fluxes dominate causing the intrusions to slope and, consequently, release potential energy.

Krishnamurti (2006) has presented measurements of a continuous interleaving set of experiments, discussing the role of the convective regions and the related Reynolds stresses on the sustainment of the horizontal mean flow. The set-up used is consistent with the basic state of the linear stability analysis of Holyer (1983). The main conclusion of this work was that the Reynolds stresses generated by convective flow are able to vertically transport horizontal momentum against the viscous fluxes, therefore maintaining the mean flow. Moreover, the observations suggested that when the interleaving reaches finite amplitude, the slope of the layers is negligible.

In this study, we extend the analysis of Krishnamurti (2006) to the case of a sharp discontinuity of the components. The present experiments are, therefore, designed with a set-up similar to the classical dam-break double-diffusive front of Ruddick & Turner (1979). The dam-break configuration is closer to the conditions found at the oceanic fronts than the continuous stratification experiments of Krishnamurti (2006). Indeed, the Krishnamurti suggested the need to investigate the case of a sharp discontinuity of the fluid properties (temperature and salt). Particle image velocimetry (PIV) is employed to measure two-dimensional flow fields. From the two-dimensional velocity fields, we can ultimately investigate the relative importance of the Reynolds stresses compared to the viscous momentum flux, on the transport of horizontal momentum. The Reynolds stresses are due to highly convective flows characterized by vortical structures at different scales. These structures are identified using a vortex identification technique based on the evaluation of the swirling strength (Chong, Perry & Cantwell 1990; Zhou *et al.* 1999; Adrian, Christensen & Liu 2000). Moreover, the budget of the mean-flow kinetic energy is also discussed. We will show that close

Experiment run	ρ/ρ_0	ΔS (g l^{-1})	ΔT (g l^{-1})	Total depth d (cm)
Experiment 1	1.0526 ± 0.0002	148	78.8	23 ± 0.2
Experiment 2	1.0526 ± 0.0002	148	78.8	23 ± 0.2
Experiment 3	1.1764 ± 0.0040	566	300	23 ± 0.2
Experiment 4	1.0195 ± 0.0001	56.5	30	23 ± 0.2
Experiment 5	1.1278 ± 0.0002	375	200	23 ± 0.2

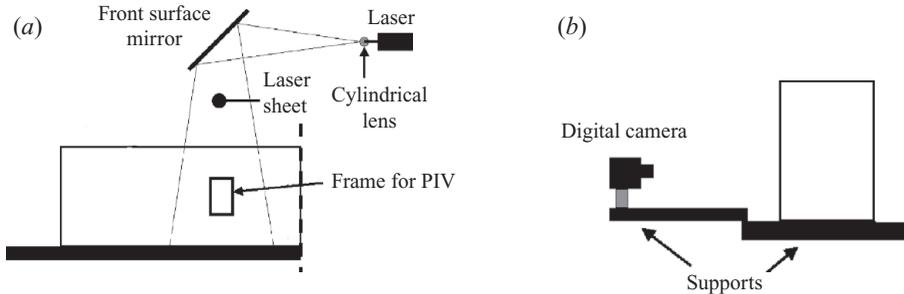TABLE 1. Main parameters of the experiments.

FIGURE 1. (*a*) Front view of half of the tank where the PIV is located together with the laser and optics. (*b*) Side view of the apparatus.

to the nose of the interleaving, the Reynolds stresses at small scales are able to sustain the mean flow. This conclusion is further supported by a spectral analysis in terms of power spectral density (PSD) as a function of the wavenumber, which suggests that kinetic energy is transferred from the small scales to the larger scales (mean flow). These kinds of processes are well documented in the literature and are often called 'negative eddy viscosity' processes (see Tsinober 2001, §8.6): they are observed wherever the Reynolds stresses have an opposite sign with respect to the mean shear. Other examples can be found in different experimental contexts, for instance the turbulent wind in Rayleigh–Bénard convection (Krishnamurti & Howard 1981), small-scale flows driven by electromagnetic forces (Paret & Tabeling 1998), and turbulent-channel flows with drag-reducing polymers (Wei & Willmarth 1992).

2. Experimental set-up and data analysis

The experimental set-up is inspired by the approach proposed by Ruddick & Turner (1979). For experimental purposes, it is possible to use a system of sugar and salt as a proxy of the natural system in which double-diffusive convection is triggered by stratification due to salt and temperature, since the ratio between the coefficients of molecular diffusivity is 1/3. Using this analogue, sugar plays the role of salt, and salt plays the role of the temperature. The working solutions are made of distilled water and sodium chloride (T) or sucrose (S). The main parameters of the experimental runs are shown in table 1.

The experiments are performed in a Perspex rectangular tank with dimensions 180 cm × 30 cm × 10 cm, placed on a rigid support, as shown in figure 1. The tank is designed with a removable partition in the central section, which initially separates the solutions. The method used to prepare the density gradients is the 'two-bucket system', which is essentially a mechanical-mixing procedure, commonly used in the

double-diffusion experiments (Ruddick & Turner 1979; Holyer *et al.* 1987). Great care is taken to minimize the density anomaly effects across the vertical interface by producing density profiles on the two side of the tank as close as possible. Moreover, to avoid pressure gradient effects, the depth has to be equal on both sides of the tank. The gate is completely removed at a very slow rate, in order to minimize any disturbances. Measurements of two-dimensional velocity fields on a vertical plane are obtained with a PIV system. We adopt a continuous green light He–Ne laser with a power of 25 mW to illuminate a portion of the tank and a high resolution still digital camera. The dimensions of the field of view of PIV images are 6.75 cm $\times$ 9 cm. The position of the measuring window is fixed and is displayed in figure 1; its position is approximately 30 cm from the removable gate. The digital image evaluation is performed by means of cross-correlation analysis. Based on our set-up, the measured velocity-vector fields have a resolution of three vectors per millimetre. This leads to a reasonable spatial resolution to describe flow structures with spatial scales of the order of a few millimetres. From the two-dimensional velocity fields, we compute horizontal averaged velocity profiles, Reynolds stresses, momentum fluxes and production and dissipation terms of the mean-flow kinetic energy budget. Moreover, we employ a vortex identification method based on the swirling strength (λ_{ci}) to reveal the presence of coherent vortical-flow structures (see Chong *et al.* 1990; Zhou *et al.* 1999; Adrian *et al.* 2000, among others). To evaluate the swirling strength in the case of two-dimensional flow fields, $\boldsymbol{u} = (u(x, z, t), v(x, z, t))$, it is necessary to compute the eigenvalues of the local velocity gradient tensor, which takes the form

$$\nabla \boldsymbol{u} = \begin{pmatrix} \partial u/\partial x & \partial u/\partial z \\ \partial v/\partial x & \partial v/\partial z \end{pmatrix}, \tag{2.1}$$

where $u(x, z, t)$ is the horizontal velocity and $v(x, z, t)$ is the vertical velocity. The characteristic equation is of second order and, therefore, the resulting two eigenvalues can be both real or complex conjugates ($\lambda_r \pm i\lambda_{ci}$). The swirling strength is defined as the positive imaginary part of the complex eigenvalue (Adrian *et al.* 2000); it measures the pure rotational velocity (swirl) of the fluid particles around the λ_r-axis in eigen-frame coordinates (Zhou *et al.* 1999). A vortex is then identified as a region of the flow with high values of λ_{ci}. Note that the swirling strength is invariant with respect to any rigid translation; therefore, a vortex moving with the mean flow is revealed without any preprocessing of the velocity fields. The swirling strength is more efficient than the vorticity to identify vortices since it is not sensitive to the mean shear.

Finally, together with velocity measurements, we have also followed the evolution of the interleaving recording pictures using the colour polarigraph technique proposed by Ruddick (1991), which is based on the ability of sugar to modify the polarization of the light depending on its concentration. The resulting images, converted to grey scale, will show darker regions where the fluid is rich in sugar, and lighter regions will correspond to layers rich in salt.

3. Experimental observations

A soon as the barrier is removed, an intruding wave-like motion is generated by the residual density mismatch across the vertical interface between the two solutions. During the very early stage of the experiment, these density currents are predominant. However, these motions rapidly die away, i.e. in less than a minute, and then the
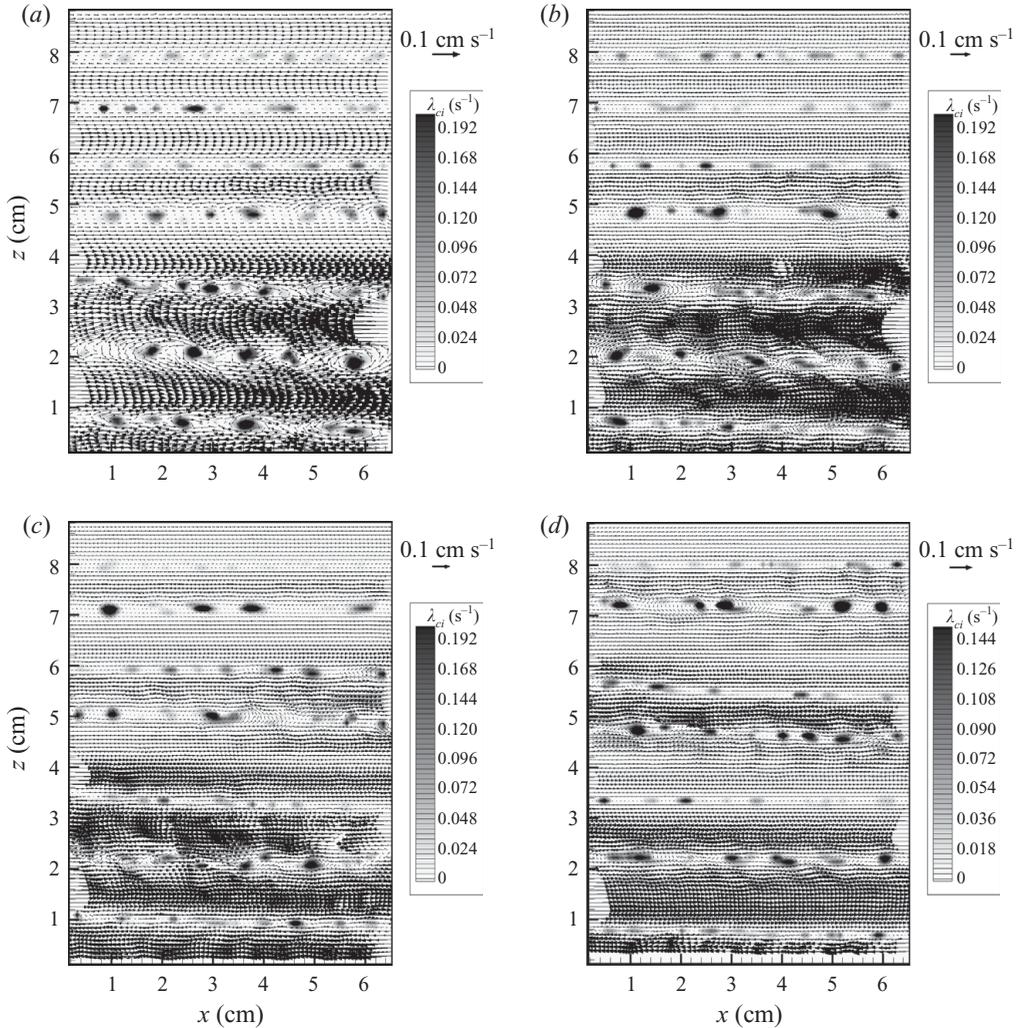
FIGURE 2. Two-dimensional velocity-vector fields at four different times of experiment 4. Time goes from (*a*) to (*d*).

diffusive processes take place, leading to the formation of the interleaving. The double-diffusive intrusions evolve with velocity around a few centimetres per minute. Typical sequences of velocity-vector fields at four different times during experiment 4 are shown in figure 2. The velocity vectors are plotted together with contours of the swirling strength λ_{ci} which help in the identification of the core of vortical structures. By inspecting these figures, regions with strong convective motions, i.e. vortical structures at different scales and with non-steady features, appear clearly. These convective regions are typically more intense near the bottom of the tank, where the salinity contrast $\beta\Delta S$ is higher. The scales of these vortices range from quite small scales up to scales comparable with the layer thickness. Similar flow structures are described in the recent work of Krishnamurti (2006), where they were visually recognized in the shadowgraphs and in the PIV fields. Moreover, a similarity can also be found in the visualizations of Tsinober, Yahalom & Shlien (1983, figure 8) and of Tanny & Tsinober (1988, figure 14).

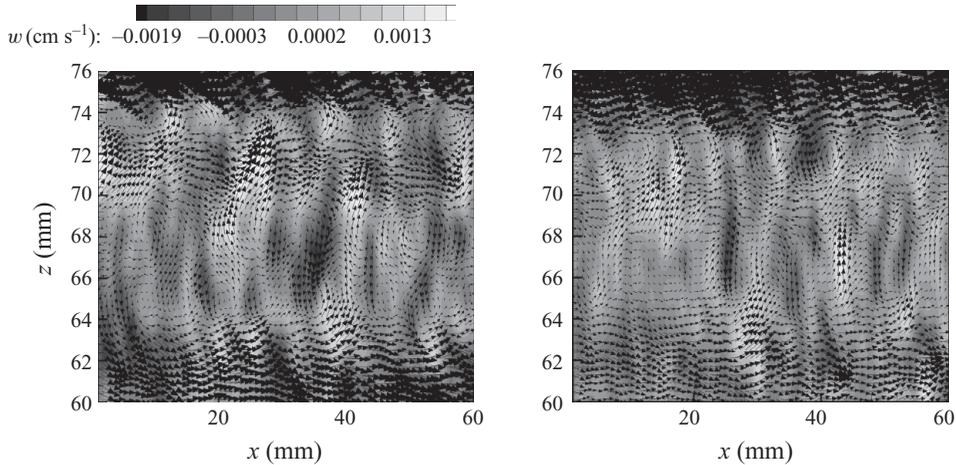$w\,(\text{cm s}^{-1})$: −0.0019   −0.0003   0.0002   0.0013

FIGURE 3. Two-dimensional flow fields showing the presence of salt fingers at two different times during experiment 5. The scales of the plot are stretched for clarity.

Since the measuring window is fixed, after a while the nose passes over the field of view of the digital camera and, then, the core of the layers can be studied. Away from the interleaving layers' nose, the flow becomes smoother and the convective activity is less and less vigorous (see figure 2*d*).

If we now look at the small-scale flows, we expect those layers with an excess of salt to be prone to generating fingers and, indeed, in the present experiments, salt fingers are observed during the evolution of the interleaving. Fingers are usually tilted with respect to the vertical and they become unstable, leading to the generation of intense convective regions. Also in the case discussed in this paper, the mean flow has the opposite directions above and below the convective flows, as revealed in the observation of Krishnamurti (2006). An example of a finger zone observed during experiment 5 is given in figure 3, where contours of the vertical velocity are superimposed on the vector fields to help the identification of the single finger cell. We estimate that the thickness of the interface is usually of the order of 1–3 cm, decreasing appreciably with time. From the behaviour of the vertical velocity, we evaluate the typical horizontal length scale of the fingers, obtaining values of a few millimetres. On the opposite side of the finger-favoured layers, the gradients of salt and sugar are present to such an extent that they excite a diffusive-like instability, which can produce either an oscillatory pattern or rolling structures. The latter is known as a travelling wave instability, which may grow in the same condition of the diffusive regime, as described in the linear stability analysis by Baines & Gill (1969). In fact, Baines & Gill (1969) have shown that an instability leading to pure oscillatory modes can arise in the first quadrant of their stability diagram in the thermal and salinity Rayleigh numbers plane. If one allows for the existence of propagating disturbances for the same Rayleigh numbers of the pure oscillatory mode, travelling waves are observed in the form of small vortices, all rotating in the same direction, which are convected by the mean flow. Theory and observations can be found in Predtenchensky *et al.* (1994), where patterns of travelling waves are recorded by the Schlieren technique. Predtenchensky *et al.* have performed a finite amplitude analysis based on a Ginzburg–Landau equation. Mapping the swirling strength, together with a simple Galilean decomposition of the flow, allows us to locate these rolling structures and its convective velocity. An example of travelling waves is shown in figure 4. The
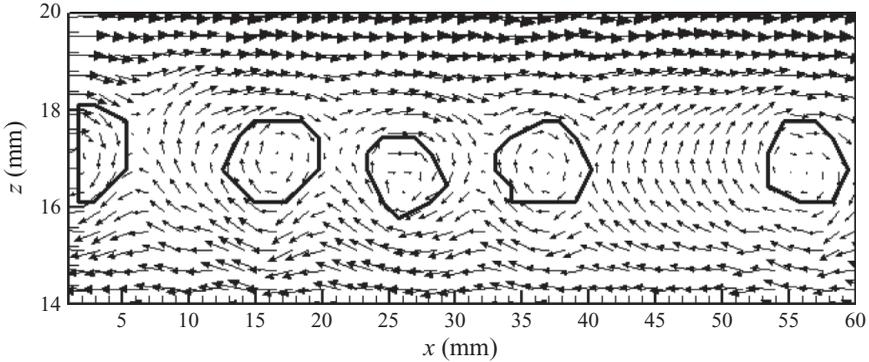
FIGURE 4. Travelling wave instability revealed by a Galilean velocity decomposition applied to a vector field of an interface between two layers. A contour of the swirling strength is plotted to emphasize the location of the rolling structure.

convective velocity of the small-scale vortices found in the vector fields is consistent, in terms of magnitude and direction, with the mean horizontal velocity of the layer with an excess of T.

Regarding the slope of the interleaving layers, the observations suggest that it tends to decrease as the layers extend laterally, leading to almost horizontal intrusions. These observations are in qualitatively agreement with those of Krishnamurti (2006).

Finally, once the intrusive noses reach the end walls of the experimental tank, typically in about 30 min, the supply of the components S and T is inhibited, after which the layers change from growing/extending to running down, causing a decrease in intensity and scales. In the present contribution the run down is not investigated.

4. Discussion of the results

A quantity that is interesting for the description of the interleaving is the mean horizontal velocity profile along the vertical direction. We introduce a decomposition of the instantaneous horizontal velocity which reads $u(x, z, t) = U(z, t) + u'(x, z, t)$, where $u(x, z, t)$ is the instantaneous horizontal velocity derived from PIV analysis, $U(z, t)$ is the horizontal velocity averaged along the x-axis and $u'(x, z, t)$ is the fluctuation of the horizontal velocity with respect to the mean. Similarly, we can define a mean vertical velocity $V(z, t)$ and its fluctuating part $v'(x, z, t)$. Examples of the computed averaged profiles of horizontal velocity are shown in figure 5 together with the corresponding distribution of the viscous stresses and the mean horizontal Reynolds stress $\overline{u'v'}$, at two different times during experiment 2: in a neighbourhood of the layer noses (see figure 5a); in the core region of the intrusions (see figure 5b). Note that the x-axis range of the panel showing the Reynolds stresses at the layer nose has been extended in order to include the higher values compared with the viscous stresses.

Averaging over the horizontal direction leaves us with a sequence of layers alternately pointing in opposite directions. However, figure 5 can be misleading when we consider the profiles of the mean velocity in regions away from the nose. In fact, to understand where a single layer extends, we need to place beside the previous figure a visualization taken of the PIV measurements at the same time (see figure 6). We remind the reader that the visualizations have been performed using the property of sugar solutions to polarize light rays; the resulting images show darker regions
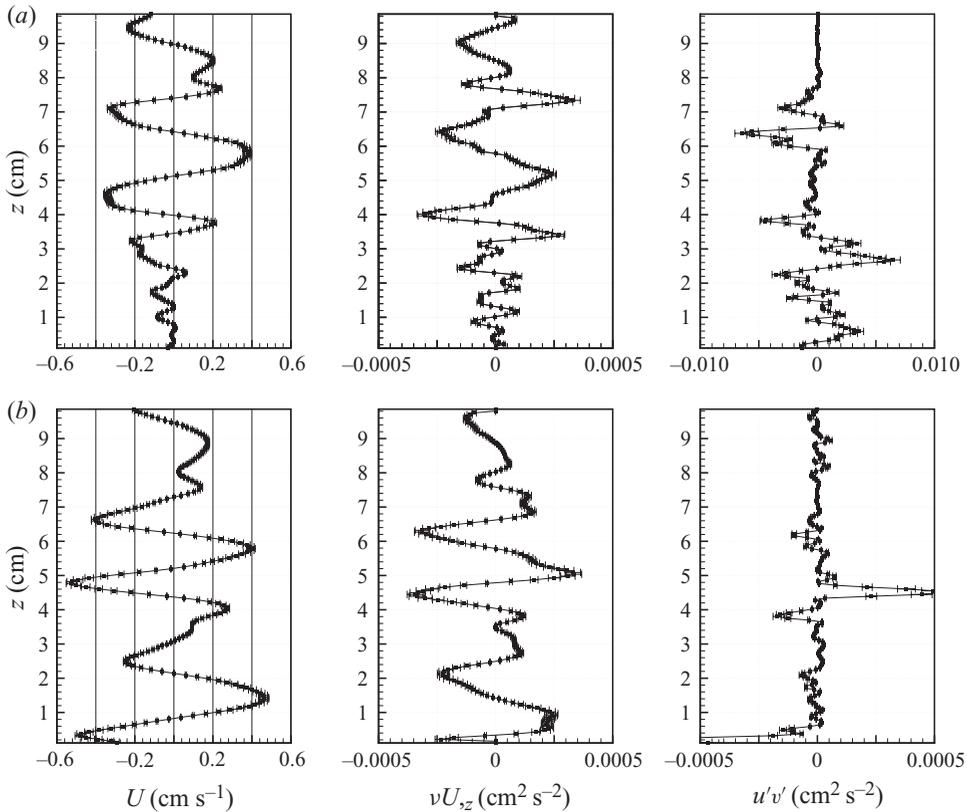
FIGURE 5. Vertical profiles of horizontal averaged velocity U, viscous stresses and Reynolds stresses for experiment 2 at two different times: (*a*) close to the nose of the layers, (*b*) inside the core of the layers. Note that to make the values of the viscosity of the Reynolds stresses readable, different ranges in the *x*-axis have been adopted for the plots.

wherever the fluid carries an excess of sugar, whereas lighter regions correspond to layers richer in salt. The mean horizontal velocity in the cores of the layers has been found to exceed the nose velocity; therefore, an intense recirculation is due to the horizontal divergence. Ruddick *et al.* (1999) have related this recirculation to the requirement that the mean salt profile spread with the noses owing to horizontal advection. By inspecting the grey-scale picture, it can be noted that the slope of the intrusion is substantially zero and, therefore, the layers grow horizontally.

The profiles reported in figure 5 show that, close to the nose of the interleaving, the Reynolds stresses largely exceed the viscous stresses, whereas inside the core of the layers the viscous stresses are comparable or even larger than the turbulent stresses. Moreover, in some regions along the vertical axis, the sign of the Reynolds stresses is opposite to the sign of the mean shear. This condition is of some interest and suggests that the Reynolds stresses may play an important role in the maintenance of the mean flow. In fact, the Reynolds stresses can couple the small-scale fluctuations with the mean flow. These kinds of phenomena are often called 'negative eddy viscosity' processes (Tsinober 2001), and observations are reported in different fields (Krishnamurti & Howard 1981; Wei & Willmarth 1992; Paret & Tabeling 1998).

We then start to discuss an analysis similar to Krishnamurti (2006), who studied the diffusive interleaving in the case of continuous horizontal gradients of T and S.
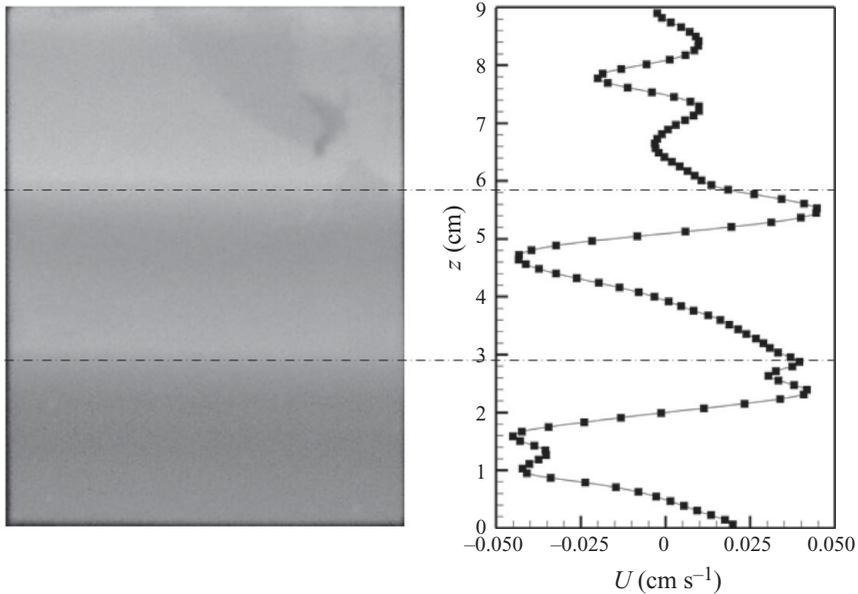
FIGURE 6. Example of a coloured visualization of the core region of the interleaving together with the corresponding velocity profiles (experiment 5); darker regions correspond to layers of fluid richer in sugar. The dot-dashed lines indicate the interfaces between layers.

In particular, assuming an unbounded longitudinal domain, the steady momentum equation along the horizontal axis can be written as (see Krishnamurti & Howard 1981; Tsinober 2001; Krishnamurti 2006, among others):

$$\frac{\partial \overline{u'v'}}{\partial z} = \nu \frac{\partial^2 U}{\partial z^2}. \tag{4.1}$$

Integrating once leads to:

$$\overline{u'v'} - \nu \frac{\partial U}{\partial z} = \text{const.} \tag{4.2}$$

where the right-hand side of the equation is independent of z.

The averaged longitudinal pressure gradient is usually not retained in the equation by Krishnamurti & Howard (1981), Tsinober (2001) and Krishnamurti (2006). In this study, we have tried to compute the intensity of the pressure term starting from the time-dependent two-dimensional velocity fields following the method proposed by Imaichi & Ohmi (1983). In fact, starting from the unsteady two-dimensional flow equation, it is possible to compute all the terms and, ultimately, deduce the values of the pressure gradients. This method has been applied in different experimental set-ups, where two-dimensional velocity measurements were performed (see Green & Gerrard 1993; Jillians & Maxworthy 1994; Guala & Stocchino 2007, among others). In this study, the values of the averaged longitudinal pressure gradient has always been found to be of the order of 10^{-6}–10^{-7} cm s^{-2} and, therefore, several orders of magnitude smaller than the divergence of the stresses, which have values of order 10^{-3} cm s^{-2}. For this reason, we have omitted the pressure term from the momentum balance.

By inspecting (4.2), it is clear that wherever, along the vertical direction, the sign of the Reynolds stresses is opposite to the sign of the viscous momentum flux, they could transport horizontal momentum vertically to the mean flow. If this is the case,
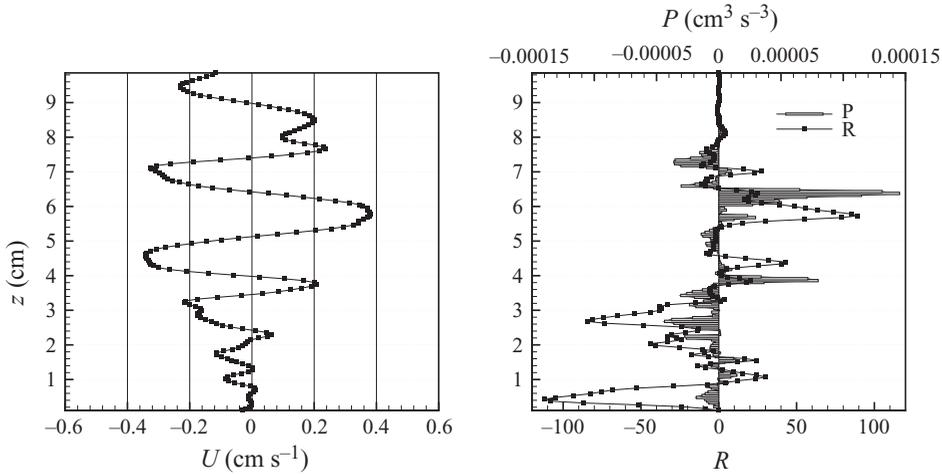
FIGURE 7. Vertical profiles of horizontal-averaged velocity and the ratio R for experiment 2 in the neighbourhood of the nose of the layers. The distribution of the turbulent kinetic energy production term P is also reported together with the stress ratio R. Note that negative values of P imply an energy transfer from the small-scale turbulent flow to the mean flow.

the interleaving can be sustained by the stresses generated by the convective motion inside the intrusions themselves. To test this hypothesis, we evaluate both terms of (4.2) and, then, we estimate the contribution of the Reynolds stresses to the transport of horizontal momentum, evaluating their ratio $R = \overline{u'v'}/(\nu \partial U/\partial z)$. Regarding the nose region, an example of a velocity profile with the corresponding distribution of the ratio between the Reynolds stresses and the viscous momentum fluxes R is shown in figure 7. In the neighbourhood of the nose, the Reynolds stresses exceed the viscous transport by two orders of magnitude, as a consequence of intense convection. The stress ratio R assumes high values for layers of considerable depth. In this case, the vertical transport of horizontal momentum owing to the Reynolds stresses is extremely efficient in the layers, where R is negative. On the contrary, the intensity of the Reynolds stresses in the core of the interleaving is much less with respect to the nose of the layers. However, the turbulent stresses still contribute to sustaining the mean recirculating flow with the layer. Values of order $O(1)$ for the ratio R are registered even if convection is much weaker. Negative eddy viscosity will imply an energy conversion that transfers kinetic energy from the small-scale turbulent flow to the larger flow scales (mean flow) (Tsinober 2001), and this should correspond to negative values of the turbulent kinetic energy term, which is the product between the Reynolds stresses and the mean shear, and reads

$$P = -\overline{u'v'}\frac{\mathrm{d}U}{\mathrm{d}z}. \tag{4.3}$$

The vertical distribution of the production term P is reported in figure 7 on the same plot of R and assumes negative values wherever R is negative-valued as well.

To explore further the physical processes that underlie the mechanism expressed by the momentum balance described above, we have performed a spectral analysis of the velocity fields for each experiment. In particular, we have computed the PSD as a function of the horizontal and vertical wavenumbers, k_x and k_z. The PSDs of the velocity components can reveal the dominant wavenumbers of flow structures and the energy processes related to the different scales. Typical examples of computed
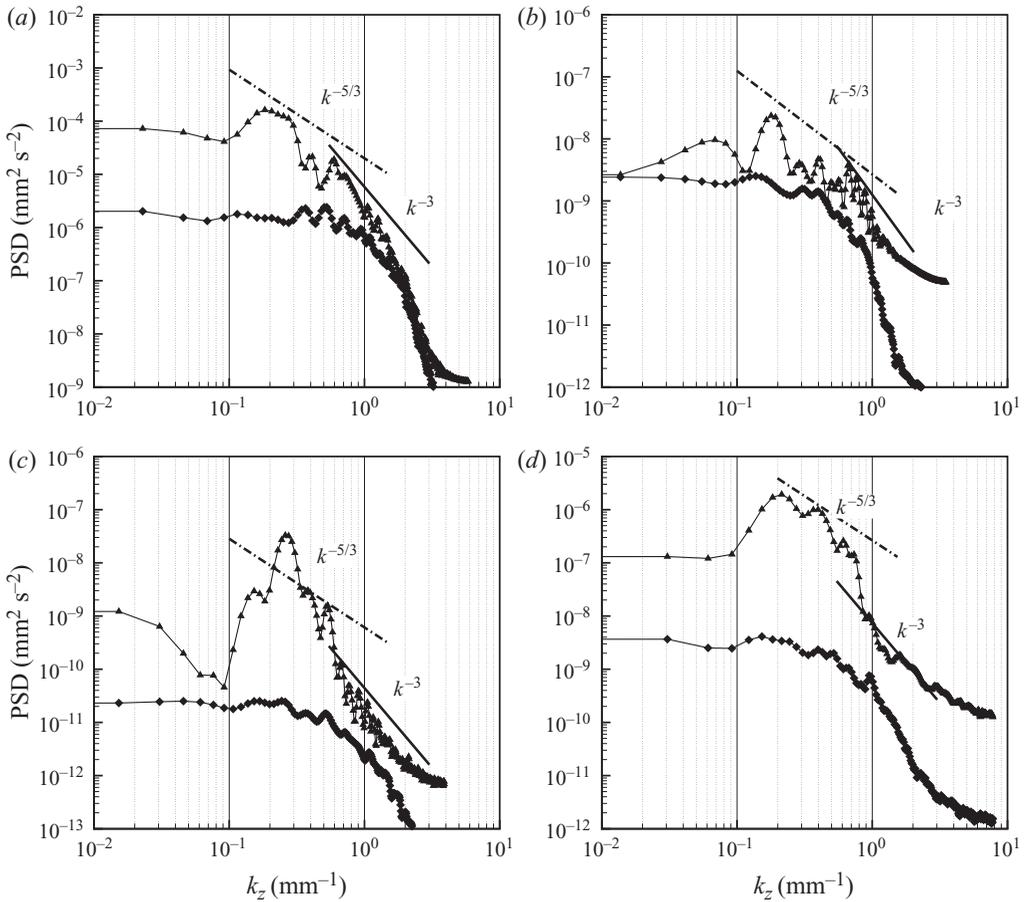
FIGURE 8. Examples of PSDs of the velocity components for different experiments: (a) experiment 2; (b) experiment 3; (c) experiment 4; (d) experiment 5. The PSDs of the longitudinal velocities u are shown with triangles, and the spectral distribution for the vertical velocity component v with diamonds.

PSDs experiments in a region close to the nose for different experiments are shown in figure 8. The energy spectra are very consistent among the different experiments and are characterized by the presence of different peaks in the wavenumbers. The main peak located for a value of the vertical wavenumber around 0.2–0.3 mm^{-1}, which corresponds to a vertical length scale of $\lambda_z = 2\pi/k_z = 20$–30 mm, can be associated with the large-scale mean-flow layers. Minor peaks are visible in a range of k_z between 0.4 and 3 mm^{-1} ($\lambda_z = 2$–15 mm) that can be related to smaller-scale convective patches in the flow. In figure 8, the power laws proportional to $k_z^{-5/3}$ and k_z^{-3} are also reported. This scaling is typical of an inverse energy cascade process, as described by Kraichnan (1976). The main consequence of an inverse energy cascade is a loss of energy of the small-scale flow at the advantage of the straining field. This mechanism is usually associated to a forced turbulence, in the sense that energy is provided at some specific wavenumbers (Kraichnan 1976). The energy supply in the case discussed in this paper is provided by the buoyancy forcing that can play the role of an external forcing for the turbulent-convective structures. By inspecting figure 8, it seems that the change in the power law occurs for wavenumbers of order 0.6–0.8 mm^{-1}. A
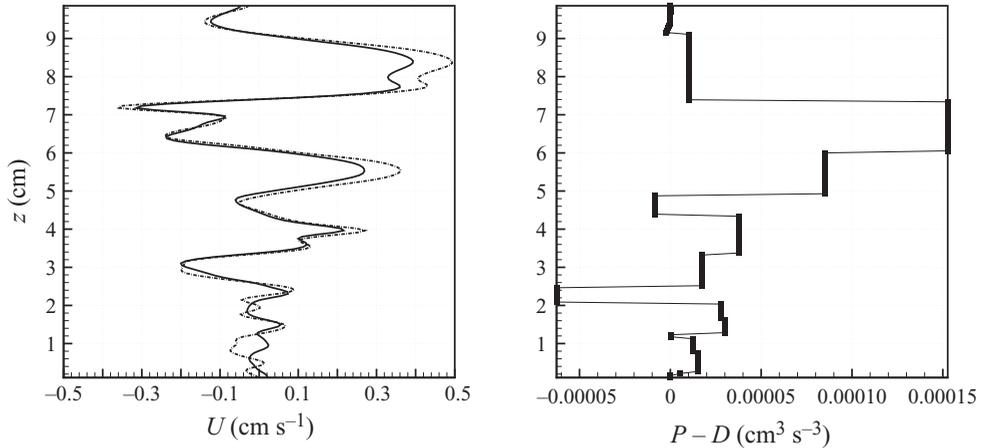
FIGURE 9. Vertical profiles of horizontal-averaged velocity at two successive times (time goes from the solid to the dotted line) and the energy balance ($P - D$) for experiment 2.

physical explanation for this value is not clear at the moment. Unfortunately, the present experimental apparatus did not allow for density measurements that would have provided valuable information on the energy source at small scales.

Finally, it is interesting to analyse the kinetic energy budget of the mean flow in order to see how the energy process described above is reflected in the mean-flow energy. From the momentum equation, using the same hypothesis assumed to obtain (4.2), the kinetic energy budget of the mean flow can be expressed in a simplified form as (Tsinober 2001; Krishnamurti 2006)

$$\frac{\partial}{\partial t} \int_{layer} \left(\frac{U^2}{2} \right) \mathrm{d}z = \int_{layer} \left(\overline{u'v'} \frac{\partial U}{\partial z} \right) \mathrm{d}z - \nu \int_{layer} \left(\frac{\partial U}{\partial z} \right)^2 \mathrm{d}z, \qquad (4.4)$$

where the integral indicates a volume average over a single layer defined by the velocity inversions (zero-crossing of the velocity profiles). The first term on the right-hand side of (4.4) represents the production (P) of the mean-flow kinetic energy, whereas the second term represents the viscous dissipation (D). Depending on the sign of P, the kinetic energy of the mean flow can be increased by the interaction between the Reynolds stresses and the mean velocity gradient, leading to an acceleration of the horizontal intrusion. This occurs as long as the sign of the Reynolds stresses is opposite to the sign of the mean shear, i.e. $R < 0$. Note that in the presence of a direct-energy cascade, the production term in the above equation is typically negative, indicating that the mean flow (large scales) is supplying energy to the smaller turbulent scales. We compute the difference between the production and the dissipation term of (4.4). An example is shown in figure 9 for experiment 2, where averaged velocity profiles at two consecutive times (from solid to dashed line) are compared with the distribution of the difference $P - D$. It can be seen that the intrusions are accelerating accordingly with a net production of kinetic energy that exceeds the viscous dissipation.

5. Conclusions

Double-diffusive interleaving has been reproduced in the case of a sharp front separating two stably stratified fluids with different distributions of T and S. The

intrusions have been followed in their evolution employing PIV techniques, from which two-dimensional vector fields at different times have been obtained on a vertical plane. The analysis of the flow maps and the derived quantities have suggested the following conclusions.

(i) The x-averaged horizontal velocity U can be efficiently sustained against the viscous dissipation by the counter-gradient transport of horizontal momentum, owing to the x-averaged Reynolds stresses $\overline{u'v'}$.

(ii) The analysis of the PSDs of the velocity components suggests that an inverse energy cascade is occurring, leading to a transfer of energy from the small-scale turbulent-convective structures to the large-scale flow. This process is typical of negative eddy viscosity phenomena.

(iii) Salt fingers are mostly observed as a transient flow structures, leading to the generation of strong convective flow structures.

(iv) The balance of the mean-flow kinetic energy is consistent with the above argument; in fact, the production term (product between the Reynolds stresses and the mean shear) can exceed the viscous dissipation, leading to an increase in the kinetic energy of the mean flow and, therefore, causing an acceleration in the intrusions.

(v) The slope of the intruding layer is found to be horizontal within the experimental accuracy.

The main limitation of this study resides in the dimensions of the measuring area, which has prevented the possibility of following the development of the interleaving for the entire duration of the experiment. In fact, it would have been interesting to have an overall measurement of an intrusion along its entire path. Nonetheless, in spite of the above limitations, we feel that a step further has been made in the direction of understanding the driving mechanisms of double-diffusive interleaving. In particular, we hope that this study may contribute to addressing at least a few of the many challenging questions raised by Ruddick (2003) in his inspiring review.

REFERENCES

ADRIAN, R. J., CHRISTENSEN, K. T. & LIU, Z.-C. 2000 Analysis and interpretation of instantaneous turbulent velocity fields. *Exp. Fluids* **29**, 275–290.

BAINES, P. G. & GILL, A. E. 1969 On thermohaline convection with linear gradients. *J. Fluid Mech.* **37**, 289–306.

CHONG, M. S., PERRY, A. E. & CANTWELL, B. J. 1990 A general classification of three-dimensional flow fields. *Phys. Fluids* **A2**, 765–777.

GREEN, R. B. & GERRARD, J. H. 1993 Vorticity measurements in the near wake of a circular cylinder at low Reynolds numbers. *J. Fluid Mech.* **246**, 675–691.

GRIFFITHS, R. W. & BIDOKHTI, A. A. 2008 Interleaving intrusions produced by internal waves: a laboratory experiment. *J. Fluid Mech.* **602**, 219–239.

GUALA, M. & STOCCHINO, A. 2007 Large-scale flow structures in particle-wall collision at low Deborah numbers. *Eur. J. Fluid Mech. B: Fluids* **26**, 511–530.

HOLYER, J. Y. 1983 Double-diffusive interleaving due to horizontal gradients. *J. Fluid Mech.* **137**, 347–362.

HOLYER, J. Y., JONES, T. J., PRIESTLEY, M. G. & WILLIAMS, N. C. 1987 The effect of vertical temperature and salinity gradients on double-diffusive interleaving. *Deep-Sea Res.* **34**, 517–530.

IMAICHI, K. & OHMI, K. 1983 Numerical processing of flow-visualization pictures: measurement of two-dimensional vortex flow. *J. Fluid Mech.* **129**, 283–311.

JILLIANS, W. J. & MAXWORTHY, T. 1994 Experiments on spin-up and spin-down on a beta-plane. *J. Fluid Mech.* **271**, 153–172.

KRAICHNAN, R. H. 1976 Eddy viscosity in two and three dimensions. *J. Atmos. Sci.* **33**, 1521–1536.

KRISHNAMURTI, R. 2006 Double-diffusive interleaving on horizontal gradients. *J. Fluid Mech.* **558**, 113–131.

KRISHNAMURTI, R. & HOWARD, L. N. 1981 Large-scale flow generation in turbulent convection. *Proc. Natl Acad. Sci.* **78**, 1981–1985.

NIINO, H. 1986 A linear stability theory of double-diffusive intrusions in a temperature-salinity front. *J. Fluid Mech.* **171**, 71–100.

PARET, J. & TABELING, P. 1998 Intermittency in the two-dimensional inverse cascade of energy: experimental observations. *Phys. Fluids* **10**, 3126–3136.

PREDTENCHENSKY, A. A., McCORMICK, W. D., SWIFT, J. B., ROSEMBERG, A. G. & SWINNEY, H. L. 1994 Travelling wave instability in sustained double-diffusive convection. *Phys. Fluids* **6**, 3923–3935.

RUDDICK, B. R. 1991 The 'colour polarigraph': a simple method for determining the two-dimensional distribution of sugar concentration. *J. Fluid Mech.* **109**, 277–282.

RUDDICK, B. 2003 Laboratory studies of interleaving. *Progr. Oceanogr.* **56**, 549–547.

RUDDICK, B. & KERR, O. 2003 Oceanic thermohaline intrusions: theory. *Progr. Oceanogr.* **56**, 483–497.

RUDDICK, B. R., PHILLIPS, O. M. & TURNER, J. S. 1999 A laboratory and quantitative model of finite-amplitude thermohaline intrusions. *Dyn. Atmos. Oceans* **30**, 71–99.

RUDDICK, B. & RICHARDS, K. 2003 Oceanic thermohaline intrusions: observations. *Progr. Oceanogr.* **56**, 499–527.

RUDDICK, B. R. & TURNER, J. S. 1979 The vertical length scale of double-diffusive intrusions. *Deep-Sea Res.* **26**, 903–913.

STERN, M. 1967 Lateral mixing of water masses. *Deep-Sea Res.* **14**, 747–753.

TANNY, J. & TSINOBER, A. B. 1988 The dynamics and structure of double-diffusive layers in sidewall-heating experiments. *J. Fluid Mech.* **196**, 135–156.

TOOLE, J. M. & GEORGI, D. T. 1981 On the dynamics and effects of double-diffusively driven intrusion. *J. Phys. Oceanogr.* **10**, 123–145.

TSINOBER, A. 2001 *An Informal Introduction to Turbulence*. Kluwer Academic.

TSINOBER, A. B., YAHALOM, Y. & SHLIEN, D. J. 1983 A point source of heat in a stable salinity gradient. *J. Fluid Mech.* **135**, 199–217.

WEI, T. & WILLMARTH, W. W. 1992 Modifying turbulent structure with drag-reducing polymer additives in turbulent channel flow. *J. Fluid Mech.* **245**, 619–641.

ZHOU, J., ADRIAN, R. J., BALACHANDAR, S. & KENDALL, T. M. 1999 Mechanisms for generating coherent packets of hairpin vortices in channel flow. *J. Fluid Mech.* **387**, 353–396.